Molecular Structural Determination of Molybdena in Different Environments: Aqueous Solutions, Bulk Mixed Oxides, and Supported MoO_3 Catalysts

Hanjing Tian, Charles A. Roberts, and Israel E. Wachs*

Operando Molecular Spectroscopy & Catalysis Laboratory, Department of Chemical Engineering, Lehigh University, Bethlehem, Pennsylvania 18015

Received: April 12, 2010; Revised Manuscript Received: July 2, 2010

UV−vis diffuse reflectance spectroscopy (DRS) and Raman spectroscopy were used to examine the electronic and molecular structures, respectively, of well-defined Mo(VI) bulk mixed oxide reference compounds ((i) isolated MoO_4 or MoO_6 monomers, (ii) dimeric $O_3Mo-O-MoO_3$, (iii) chains of alternating MoO_4 and MoO_6 units, (iv) MoO_6-coordinated Mo_7-Mo_{12} clusters, and (v) infinite layered sheets of MoO_5 units), aqueous molybdate anions as a function of solution pH, and supported MoO_3 catalysts (MoO_3/SiO_2, MoO_3/Al_2O_3, and MoO_3/ZrO_2). Raman spectroscopy confirmed the identity and phase purity of the different bulk and solution molybdenum oxide structures. UV−vis DRS provided the corresponding electronic edge energy (Eg) of the ligand-to-metal charge transfer (LMCT) transitions of the Mo(VI) cations. A linear inverse correlation was found between Eg and the number of bridging Mo−O−Mo covalent bonds around the central Mo(VI) cation. A relationship between Eg and the domain size (N_{Mo}) for finite MoO_x clusters, however, was not found to exist. Application of the above insights allowed for the determination of the molecular structures of the two-dimensional surface MoO_x species present in supported MoO_3 catalysts as a function of environmental conditions. The current electronic and molecular structural findings are critical for subsequent studies that wish to establish reliable structure−activity/selectivity relationships for molybdenum oxide catalysts, especially supported MoO_3 catalysts.

1. Introduction

Molybdates are extensively applied as heterogeneous catalysts.[1] Bulk and supported molybdena catalysts are commercially employed for methanol oxidation to formaldehyde; selective oxidation/ammoxidation of propylene to acrolein, acrylic acid, and acrylonitrile; isomerization; hydrogenation; polymerization; and hydrodesulfurization (HDS) of petroleum feedstocks. In the past few years, there has also been much interest and activity in extending the use of Mo-containing catalysts to selective oxidation of lower alkanes.[2−5] Furthermore, Mo-containing heteropoly compounds with Keggin/Anderson structures were also intensively investigated due to their special redox/acidic catalytic properties in homogeneous (electrochemical and photochemical reactions), heterogeneous liquid-phase processes, and heterogeneous gas−solid reactions.[6−9]

The molybdenum oxide molecular structures in these molybdena-containing catalysts have been extensively investigated with many characterization techniques: Raman spectroscopy, Fourier transform infrared (FT-IR) spectroscopy, X-ray diffraction (XRD), solid-state ^{95}Mo nuclear magnetic resonance (NMR), XANES/EXAFS, X-ray photoelectron spectroscopy, and UV−visible diffuse reflectance spectroscopy (DRS).[9−20] These investigations have resulted in major contributions to both fundamental research and industrial catalyst development, particularly in the field of petroleum chemistry. For supported molybdena catalysts, it is generally accepted that the structure of the surface molybdena is controlled by both the specific oxide support and the surface coverage. At low surface coverage, the primary molybdena species supported on Al_2O_3, TiO_2, and ZrO_2 are isolated and tetrahedral coordinated under dehydrated conditions. At high surface coverage, the primary dehydrated molybdena species supported on Al_2O_3 and ZrO_2 are a mixture of tetrahedral and octahedral MoO_x coordinated species.[21−42] There is still, however, a lack of general understanding of the factors controlling the dispersion and local MoO_x coordination/structure of supported molybdena oxides and their dependence on the nature of supports, surface coverage, and the extent of surface hydration/dehydration.

UV−vis−NIR spectroscopy is one of the most versatile spectroscopic technique because it can function under ambient, dehydrated, and in situ conditions and measures the electron transition of the ligand-to-metal charge transfer (LMCT) in the ultraviolet (UV), visible (vis), and near-infrared (NIR) regions.[43] Furthermore, the UV−vis edge energy (Eg) or band gap of the LMCT, which is determined from the position of the low energy rise in the material's UV−visible spectrum, can also quantitatively establish the extent of polymerization of metal oxides. In recent years, therefore, UV−vis−NIR spectroscopy has found more use in the structural determination of MoO_x clusters.[2,10,26,44−47] Few publications, however, have quantitatively investigated the local Mo structure on the basis of the UV−vis edge energy values. A pioneering study was reported by R. S. Weber where the edge energies of bulk molybdenum polyoxometalates were correlated with the degree of aggregation/polymerization (calculated as the average number of nearest molybdenum neighbors).[48] Unfortunately, application of this aggregation−edge energy relationship to determine the local Mo oxide structure was problematic because (1) the data employed by Weber were collected from a number of different research groups' publications and, consequently, lacked internal consistency, (2) other characterization methods were not used to confirm the assigned molecular structures, and (3) the Eg values tend to only provide an average value when multiple molecular MoO_x species are

* Corresponding author. Phone: (610) 758-4274. Fax: (610) 758-5057. E-mail: iew0@lehigh.edu.

10.1021/jp103269w
Published on Web 08/02/2010

present.[43,48] Thus, other molecularly sensitive characterization methods must also be used in conjunction with UV−vis spectroscopic measurements to check the structural purity of MoO_x species.

The molecular structures of the different Mo(VI) oxide species present in various model compounds and environments, aqueous solution, bulk mixed oxides, supported molybdena on oxide supports under hydrated and dehydrated conditions, and Keggin polyoxometalates, will be examined with combined in situ Raman and UV−vis−NIR spectroscopy. The local molecular structure of the molybdena species will first be determined with Raman spectroscopy because of its high sensitivity in discriminating among different structures under ambient and dehydrated conditions. An empirical correlation between the size of Mo oxide domain and Eg values will be established and used to determine the local molybdena structures of supported molybdena catalysts on various oxide supports as a function of Mo loading under ambient and dehydrated conditions. Finally, the assigned structures of the supported molybdena catalysts from UV−vis spectroscopy will be compared to the corresponding Raman and XANES findings to determine the consistency of the structural assignments with these spectroscopic techniques and to provide a complete view of the molybdenum oxide structure, its dependence on various phases (solid, aqueous solution, or Keggin clusters), oxide support and dispersion, as well as the effect of surface hydration and dehydration.

2. Experimental Section

2.1. Molybdate Synthesis. The bulk metal molybdates ($Al_2(MoO_4)_3$, $MgMo_2O_7$, $Fe_2(MoO_4)_3$, Na_2MoO_4, and $NiMoO_4$) were prepared by coprecipitation of aqueous $(NH_4)_6Mo_7O_{24}\cdot 4H_2O$ (Alpha Aesar Products, 99.9%) and the corresponding metal nitrates $Al(NO_3)_3\cdot 9H_2O$, $Mg(NO_3)_2\cdot 6H_2O$, $Fe(NO_3)_3\cdot 9H_2O$, and $NaNO_3$, $Ni(NO_3)_2\cdot 6H_2O$ from Alpha Aesar Products, 99.9%). The preparation details have been previously reported.[49,50] The $(NH_4)_2Mo_2O_7$, $(NH_4)_6Mo_7O_{24}$, and $(NH_4)_4Mo_8O_{26}$ salts were obtained from H. C. Starck.

The aqueous molybdate solutions were prepared from a 0.2 M (Mo) ammonium heptamolybdate solution of doubly distilled, deionized water. The solution pH was adjusted from 2.0−11.0 by addition of appropriate amounts of acidic 1 M HCl and basic $NH_4\cdot H_2O$. Measurements of the pH were required during synthesis as well as during the several of the experimental procedures. The pH of the aqueous solutions was measured using a Cole Parmer pH/mV/°C meter, and the electrode was standardized using pH solutions of 4, 7, and 10.

The supported molybdena catalysts on Al_2O_3 (Engelhard, 180 m^2/g), SiO_2 (Cabosil, 380 m^2/g), and ZrO_2 (Degussa, 39 m^2/g) were prepared by incipient-wetness impregnation with aqueous solutions of ammonium heptamolybdate ($(NH_4)_6Mo_7O_{24}\cdot 4H_2O$, Alpha Aesar Products, 99.9%) as previously described.[23] After impregnation, the samples were dried overnight under ambient conditions and subsequently calcined in dry air (AirGas, ultrahigh purity (UHP) air) at 723 K for 2 h. The molybdenum oxide loading of the catalysts is given as the nominal weight percent of the MoO_3 in the samples.

2.2. BET Surface Area. The BET surface areas were measured with the N_2 adsorption/desorption method with a Quantachrome QT-3 BET system. The BET surface areas of the samples were obtained using a 3:7 ratio of N_2/He mixture. Typically, 0.200−0.300 g of sample was used for the measurement, and the sample was outgassed prior to N_2 adsorption.

2.3. UV−Vis Diffuse Reflectance Spectroscopy (DRS). The UV−vis DRS measurements were performed with a Varian Cary 5E UV−vis spectrophotometer with the diffuse reflectance integration sphere attachment. Finely ground powder samples of bulk or supported MoO_x catalysts were loaded into an environmental cell (Harrick, HVC-DR2), and the UV−vis spectra were collected in the 200−800 nm region. An MgO reflectance standard was used as the baseline. The spectra of the dehydrated samples were obtained at room temperature after the samples were heated to 400 °C in flowing 10% O_2/He gas (Air Gas, UHP certified gas mixture) at 30 mL/min for 1 h.

The darker colored $Fe_2(MoO_4)_3$ and $NiMoO_4$ bulk mixed-metal molybdates were diluted with the MgO white standard to minimize the effects of regular reflection and particle size. The MgO was added until the Kubelka−Munk $F(R_\infty)$ function became less than 1 and a constant UV−vis DRS edge energy resulted.

The UV−vis DRS measurements of the aqueous molybdate solutions were also obtained in the 200−800 nm range. In the double beam mode, the UV−vis radiation passed though the first quartz cell containing the aqueous molybdate solution, and a second quartz cell containing only reference water with the same path length was also simultaneously monitored.

The Kubelka−Munk $F(R_\infty)$ function was calculated from the absorbance of the UV−vis DRS. The edge energy (Eg) for allowed transitions was determined by finding the intercept of the straight line for the low-energy rise of a plot of $[F(R_\infty)h\nu]^2$ versus $h\nu$, where $h\nu$ is the incident photon energy.[51] A graph containing an example of the determination of Eg can be found in Figure S1.

2.4. Raman Spectroscopy. The Raman spectra were collected with a state-of-the-art combined UV/visible Raman spectrometer system (Horiba-Jobin Yvon LabRam-HR) equipped with a confocal microscope (Olympus BX-30), notch filter (532 nm), single stage monochromator, and a 900 grooves/mm grating. The visible laser excitation at 532 nm (green) was supplied by a Yag doubled diode pumped laser (20 mW, manufacturer's specifications). The scattered photons were directed and focused onto the single stage monochromator and measured with a UV sensitive LN_2-cooled CCD detector (Horiba-Jobin Yvon CCD-3000 V). The notch filter has a ~100 cm^{-1} cutoff for the visible spectra, thus only allowing Raman spectral collection above 100 cm^{-1}. The spectral resolution of the Horiba-Jobin Yvon LabRam-HR system is better than 2 cm^{-1} for the given parameters.

The various aqueous molybdate solutions were deposited on glass slides placed below the confocal microscope to obtain their Raman spectra. Similarly, the Raman spectra of the ambient MoO_x-containing catalysts were also collected by loosely spreading the powder onto glass slides. The Raman spectra of the dehydrated MoO_x-containing catalysts were obtained by loading ~30 mg of finely ground sample into an environmental cell (Linkam, TS1500) and dehydrating at 400 °C for 1 h in flowing 10% O_2/He (30 mL/min) to remove the adsorbed moisture. The Raman spectra of the dehydrated MoO_x-containing catalysts were collected at room temperature in the flowing 10% O_2/He. The laser power was typically kept below 0.5 mW at the samples to minimize any laser-induced sample changes. Spectral collection times were typically 2−5 s per scan with two scans.

3. Results

3.1. Bulk Molybdate Compounds. The Raman spectra of the various bulk metal molybdate compounds with known structures, under ambient conditions, are shown in Figures 1

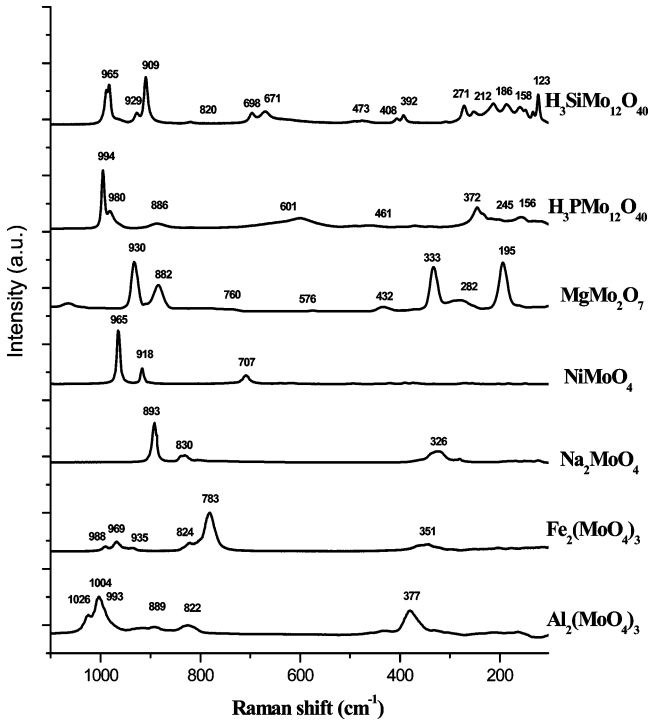

Figure 1. Raman spectra of various bulk metal molybdate compounds.

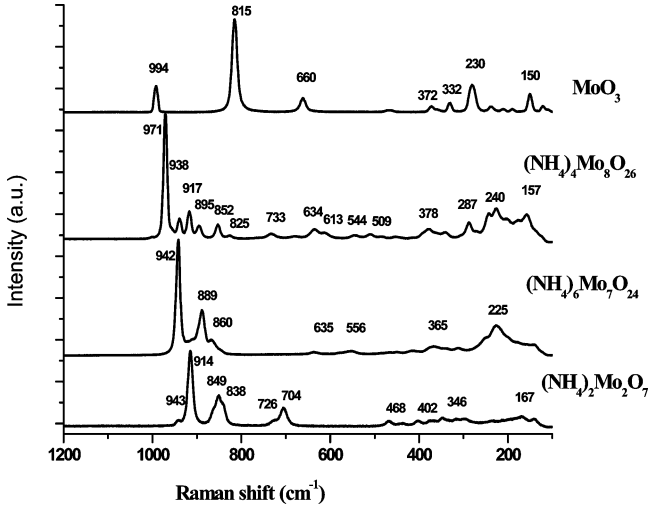

Figure 2. Raman spectra of ammonium molybdate salts and α-MoO_3.

and 2. Their corresponding UV−vis DRS edge energy values, local coordination, and molecular structures are summarized in Table 1.

Isolated MoO_4 Structures. Only isolated MoO_4 sites are present in the bulk $Fe_2(MoO_4)_3$,[52−56] $Al_2(MoO_4)_3$,[52,57−59] and Na_2MoO_4[60,61] compounds. The appearance of triplet bands in the 930−1030 cm^{-1} region of the Raman spectra of $Al_2(MoO_4)_3$ (1026, 1004, and 993 cm^{-1}) and $Fe_2(MoO_4)_3$ (988, 969, and 935 cm^{-1}) reflects the presence of three highly distorted MoO_4 units in these compounds. The distortion of the MoO_4 unit refers to a deviation in ideal structure corresponding to a shortening of the Mo−O bonds, which is manifested in Mo−O vibrations at higher wavenumber Raman shifts. In contrast, bulk Na_2MoO_4 exhibits only a single Raman band at 922 cm^{-1}, reflecting the presence of only one MoO_4 unit with a less distorted structure because lower wavenumber values correspond to longer Mo−O bonds.[52] Furthermore, the absence of Raman bands in the 500−700 cm^{-1} range further confirms that the MoO_4 units in the bulk $Fe_2(MoO_4)_3$, $Al_2(MoO_4)_3$, and Na_2MoO_4 compounds are isolated and free of Mo−O−Mo bridging bonds. The high UV−vis DRS Eg values of these three compounds (4.2−4.7 eV) reflect the isolated nature of these MoO_4 containing structures. The Eg values also vary inversely with extent of distortion (e.g., $Al_2(MoO_4)_3$ contains the most distorted structure with an Eg = 4.2 eV, the intermediately distorted $Fe_2(MoO_4)_3$ exhibits an Eg = 4.5 eV, and the least distorted Na_2MoO_4 possesses an Eg = 4.7 eV).

TABLE 1: Bulk Molybdena Local MoO_x Structures and Corresponding UV−Vis DRS Edge Energy (Eg) Values

bulk MoO_x compound	local MoO_x structure	Eg (eV)
$Al_2(MoO_4)_3$	isolated MoO_4	4.2
$Fe_2(MoO_4)_3$	isolated MoO_4	4.5
Na_2MoO_4	isolated MoO_4	4.7
$NiMoO_4$	isolated MoO_6	4.4
$MgMo_2O_7$	Mo_2O_7 dimer	4.2
$(NH_4)_2Mo_2O_7$	alternating MoO_4/MoO_6linear chain	3.5
$(NH_4)_6Mo_7O_{24}$	MoO_6-containing cluster	3.5
$(NH_4)_4Mo_8O_{26}$	MoO_6-containing cluster	3.4
$H_3PMo_{12}O_{40}$	MoO_6-containing cluster	2.7
α-MoO_3	infinite layered sheets	3.5

Isolated MoO_6 Structures. Only isolated, distorted MoO_6 sites are present in bulk $NiMoO_4$,[52,62−65] and the Raman band at 965 cm^{-1} is assigned to the MoO_6 symmetric stretch, and bands at 918 and 707 cm^{-1} are attributed to the corresponding MoO_6 asymmetric vibrations. The absence of Raman bands in the 500−700 cm^{-1} range reflects the lack of bridging Mo−O−Mo bonds and further confirms the isolated structure of the MoO_6 units in bulk $NiMoO_4$. The corresponding UV−vis DRS Eg value of the isolated MoO_6-containing $NiMoO_4$ compound occurs at 4.4 eV, which is comparable to that found for the distorted bulk $Fe_2(MoO_4)_3$ and $Al_2(MoO_4)_3$ compounds containing only isolated MoO_4 units.

Dimeric Mo_2O_7 Structure. The dimeric $O_3Mo−O−MoO_3$ unit is present in the bulk $MgMo_2O_7$ compound.[60,61,66,67] The Raman spectrum of $MgMo_2O_7$ exhibits strong bands at 930 and 882 cm^{-1}, which are assigned to the symmetric and asymmetric MoO_4 stretches, weak and broad bands at 476 and 706 cm^{-1} (symmetric and asymmetric stretches of bridging Mo−O−Mo bonds, respectively), and bands at 333 and 195 cm^{-1} (bending modes of the MoO_4 unit and the bridging Mo−O−Mo bond, respectively). The corresponding UV−vis DRS Eg value of $MgMo_2O_7$ occurs at 4.2 eV, which is lower than the Eg values found for the isolated MoO_4/MoO_6 units in the bulk compounds above with the exception of the highly distorted MoO_4 units present in bulk $Al_2(MoO_4)_3$.

Linear Mo_2O_7 Chains. Linear Mo_2O_7 chains consisting of alternating MoO_4/MoO_6 units are contained in the bulk $(NH_4)_2Mo_2O_7$ salt.[68,69] The strong Raman bands at 943 and 914 cm^{-1} are assigned to the symmetric stretching modes of the MoO_4 and MoO_6 units, respectively, and the weak, overlapping bands at 849 and 838 cm^{-1} are assigned to the corresponding asymmetric stretches, respectively. The presence of bridging Mo−O−Mo bonds is clearly reflected by the Mo−O−Mo stretches at 470 and 704/724 cm^{-1} as well as Mo−O−Mo bending mode at 167 cm^{-1}. The weak Raman band at 315 cm^{-1} is assigned to the symmetric/asymmetric bending modes of the MoO_4/MoO_6 units. The corresponding Eg value for the $(NH_4)_2Mo_2O_7$ salt containing a linear MoO_x polymeric chain is 3.5 eV, which is significantly below that for dimeric Mo_2O_7 (Eg = 4.2 eV).

Mo_7O_{24} Cluster. The Mo_7O_{24} cluster possesses seven vertex-, edge-, corner-shared MoO_6 coordinated units in the bulk $(NH_4)_6Mo_7O_{24}$ salt.[60,70] The strong Raman band at 942 cm^{-1} is assigned to the symmetric vibration of the distorted MoO_6 units, and the weaker Raman bands at 889 and 860 cm^{-1} are associated with the asymmetric stretches. The small Raman bands at 556 and 635 cm^{-1} are associated with the asymmetric and symmetric vibrations of the bridging Mo−O−Mo bonds, and the bands at 200−400 cm^{-1} are related to the bending modes. The corresponding UV−vis DRS Eg value for the Mo_7O_{24} cluster in the $(NH_4)_6Mo_7O_{24}$ salt is 3.5 eV, which is comparable to the Eg value for the linear MoO_4/MoO_6 chain structure present in $(NH_4)_2Mo_2O_7$.

Mo_8O_{26} Cluster. The Mo_8O_{26} cluster is composed of eight MoO_6 octahedra with six of the MoO_6 octahedra arranged in the same way as in Mo_7O_{24} cluster.[71−73] The Raman spectrum of $(NH_4)_4Mo_8O_{26}$ possesses a symmetric stretch at 971 cm^{-1} from the distorted MoO_6 unit and several weaker bands at 822−941 cm^{-1} from the related asymmetric stretches. The weak Raman bands at 544, 613, 634, and 733 cm^{-1} originate from the symmetric and asymmetric stretches, and the corresponding band at 157 cm^{-1} is from the symmetric bending mode of the bridging Mo−O−Mo bonds. The asymmetric and symmetric bending modes of the MoO_6 unit occur at 340 and 400 cm^{-1}. The multitude of features in the Raman spectrum for this compound can be attributed to possible impurities of Mo_7O_{24} clusters as many of the bands overlap in the two spectra. The $[NH_4]^+$ vibrations are not observed below 1200 cm^{-1}, and every Mo atom is completely surrounded by oxygen within the cluster, which eliminates the possibility of N−Mo and N−Mo−N bonds arising from the presence of ammonium. The corresponding UV−vis Eg value for the Mo_8O_{26} cluster in the $(NH_4)_4Mo_8O_{26}$ salt occurs at 3.4 eV, which is slightly lower than that found for the Mo_7O_{24} cluster.

$Mo_{12}O_{40}$ Cluster. The $Mo_{12}O_{40}$ clusters are present in Keggin polyoxo metalate anions with the general formula $[XMo_{12}O_{40}]^{3-}$. The Keggin anion structure is composed of a globular cluster of vertex- and edge-shared MoO_6 units that enclose a central XO_4 cavity, where X can be P, Si, Al, etc. Each MoO_6 unit also contains one terminal Mo═O bond and four bridging Mo−O−Mo bonds. The MoO_6 units are edge-shared into four Mo_3O_{13} groups possessing C_{3v} symmetry, and these "ligands" are connected to the central XO_4 tetrahedron to give the overall T_d symmetry of the Keggin anion.[6−8] Some of the Raman vibrational assignments of Keggin anions are still not completely resolved in the literature; nevertheless, the Raman assignments for $H_3XMo_{12}O_{40}$ (X = P, Si) are tentatively undertaken on the basis of the empirical Raman cm^{-1} Mo−O bond length relationship[52] and DFT calculations.[74−76] The Raman spectrum of the Keggin possesses bands at 960−1000 cm^{-1} (symmetric MoO_6 stretch), 840−930 cm^{-1} (asymmetric MoO_6 stretch), 470 and 750 cm^{-1} (symmetric and asymmetric stretch of bridging Mo−O−Mo, respectively), asymmetric MoO_6 bending modes in the 500−310 cm^{-1} region, and a symmetric bending mode in the 300−100 cm^{-1} region. The UV−vis DRS Eg value for the $H_3PMo_{12}O_{40}$ Keggin anion is 2.7 eV, which is much lower than the value for the Mo_8O_{26} cluster.

Infinite Layered Sheets. Infinite layered sheets of edge-shared MoO_6 coordinated units, sometimes referred to as MoO_5 units because the sixth O atom is very far away, with weak bonding between the terminal Mo═O functionality in one layer and Mo in the adjacent layer, make up the crystalline structure of bulk α-MoO_3.[60,77,78] The modest Raman band at 994 cm^{-1} is related to the symmetric stretch of the terminal Mo═O bond, and the strong band at 815 cm^{-1} has been assigned to the asymmetric vibration of the bridging Mo−O−Mo bonds, and the associated Mo−O−Mo bending mode appears at 150 cm^{-1}. The corresponding UV−vis DRS Eg value for α-MoO_3 was determined to be 3.5 eV.

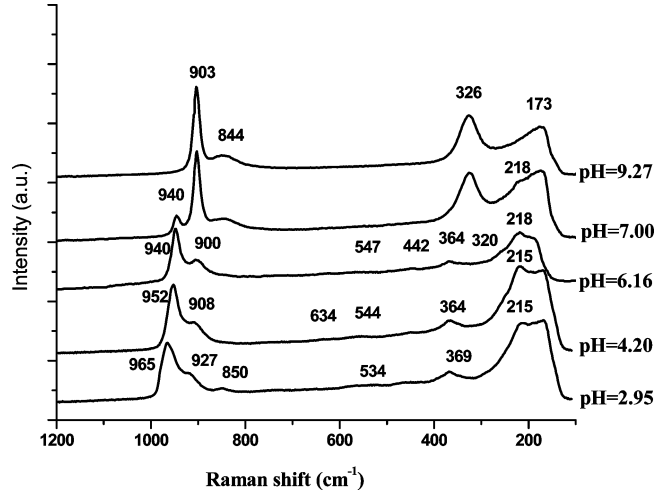

Figure 3. Raman spectra of aqueous 0.2 M $(NH_4)_6Mo_7O_{24}$ solutions as a function of solution pH. Note the 173 cm^{-1} band is from the glass dish used to hold the aqueous molybdena solution.

TABLE 2: Aqueous Solution MoO_x Structures, Determined with Raman and UV−Vis DRS Eg Values as a Function of Solution pH (0.2 M $(NH_4)_6Mo_7O_{24}$ Aqueous Solution)

aqueous pH	aqueous MoO_x molecular structure	Eg (eV)
2.95	$[Mo_8O_{26}]^{4-}$	3.4
4.2	$[Mo_7O_{24}]^{6-}+[Mo_8O_{26}]^{4-}$	3.4
6.16	$[Mo_7O_{24}]^{6-}$	3.5
7	$[MoO_4]^{2-}+[Mo_7O_{24}]^{6-}$	3.8
>9.27	$[MoO_4]^{2-}$	4.5

3.2. Aqueous Polymolybdates as a Function of Solution pH. The aqueous phase diagram for polymolybdate species reveals that three distinct aqueous molybdena species ($[MoO_4]^{2-}$, $[Mo_7O_{24}]^{6-}$, and $[Mo_8O_{26}]^{4-}$) are present and that their relative concentrations depend on both the solution pH and the MoO_x concentration.[79,80] In the present investigation, the pH of a 0.2 M $(NH_4)_6Mo_7O_{24}$ aqueous solution was varied by addition of appropriate amounts of acidic HCl and basic NH_4OH. Raman spectroscopy was initially employed to determine the aqueous molybdena speciation because of the ability of Raman to discriminate between the different aqueous molybdena molecular structures, and the corresponding Eg values were obtained with UV−vis DRS.

The Raman spectra of the aqueous 0.2 M $(NH_4)_6Mo_7O_{24}$ solution at various pH values (2.95, 4.20, 6.16, 7.00, and 9.27) are presented in Figure 3, and the corresponding molecular speciation and UV−vis DRS values are summarized in Table 2. The 173 cm^{-1} Raman band is not related to the aqueous molybdena anions and originates from the glass slide used to hold the aqueous solutions. At solution pH values of 9.27 and greater, only the isolated $[MoO_4]^{2-}$ anion is present in the aqueous solutions. The aqueous $[MoO_4]^{2-}$ anion gives rise to Raman bands at 904 and 844 cm^{-1} from the MoO_4 unit symmetric and asymmetric stretches, and 326 cm^{-1} from the related MoO_4 bending mode.[13] No vibrations characteristic of bridging Mo−O−Mo bonds are present in the 500−800 and 100−300 cm^{-1} regions of the Raman spectrum. The corresponding UV−vis DRS Eg value for the aqueous isolated $[MoO_4]^{2-}$ anion is 4.5 eV, which is consistent with the value

TABLE 3: BET Surface Area, Molybdenum Oxide Loading, and Surface Molybdena Coverage for the Supported MoO_3 Catalysts

catalysts	surface areas of the support (m^2/g)	loading weight (%)	surface density (Mo atoms/nm^2)	fraction of monolayer coverage
MoO_3/SiO_2	380	1	0.16	0.20 of maximum dispersion[a]
		5	0.80	maximum dispersion[a]
MoO_3/Al_2O_3	180	1	0.23	0.05
		20	4.6	1.0
MoO_3/ZrO_2	39	0.5	0.55	0.13
		4	4.3	1.0

[a] Maximum dispersion refers to the highest dispersion on SiO_2 before the formation of crystalline MoO_3NPs, which only occurs below monolayer coverage on SiO_2.

for isolated MoO_x units in the mixed-metal molybdate compounds (see Table 1). New Raman bands appear at 940 and 218 cm^{-1} upon lowering the solution pH to 7.0, which suggests the presence of a new aqueous molybdena species in addition to the aqueous $[MoO_4]^{2-}$ anion. As the solution pH value is lowered to 6.16, the Raman vibrations of the aqueous isolated $[MoO_4]^{2-}$ anion are no longer present, and new Raman bands associated with the aqueous $[Mo_7O_{24}]^{6-}$ anion cluster are present: 940 cm^{-1} (MoO_6 unit symmetric stretch), 900 cm^{-1} (MoO_6 unit asymmetric stretch), a very weak band at 547 cm^{-1} (symmetric stretch of bridging Mo−O−Mo bonds), 442 and 366 cm^{-1} (MoO_6 unit asymmetric and symmetric bending modes, respectively), and 218 cm^{-1} (bending mode of the bridging Mo−O−Mo bonds).[13] The corresponding UV−vis DRS Eg value is 3.5 eV for the aqueous $[Mo_7O_{24}]^{6-}$ anion and is the exact same value as the Mo_7O_{24} cluster in the ammonium salt (see Table 1). Further lowering the aqueous solution pH value to 4.20 shifts the strongest Raman band from 940 to 952 cm^{-1}, which indicates the presence of a new aqueous molybdena anion species. At an aqueous solution pH value of 2.95, only the Raman bands of the aqueous $[Mo_8O_{26}]^{4-}$ anion are present: MoO_6 unit symmetric stretch at 965 cm^{-1}, MoO_6 unit asymmetric stretching modes at 927 and 850 cm^{-1}, symmetric stretch of the bridging Mo−O−Mo bond at 534 cm^{-1}, bending mode of the MoO_6 unit at 369 cm^{-1}, and the bridging Mo−O−Mo bending mode at 215 cm^{-1}.[13] The corresponding UV−vis Eg value for the aqueous $[Mo_8O_{26}]^{4-}$ anion at 3.4 eV is identical to the Eg value for the Mo_8O_{26} cluster in the ammonium salt (see Table 1). The Raman spectra of the aqueous molybdena cluster anions are very similar to their corresponding ammonium salts, with the weak vibrations of the bridging Mo−O−Mo bonds better resolved in the ammonium salts and mixed-metal molybdate compounds.

3.3. Supported MoO_3 Catalysts. The molybdenum oxide weight loadings and surface coverage of the supported MoO_3 catalysts on the different oxide supports are summarized in Table 3. Note that it is not possible to form a complete surface MoO_x monolayer on the relatively inert SiO_2 support, and the maximum dispersion achieved in this study was 5% MoO_3/SiO_2.[81] The Raman spectra of the supported MoO_3 catalysts on SiO_2, Al_2O_3, and ZrO_2 under ambient and dehydrated conditions are shown in Figures 4−6, and the corresponding UV−vis DRS Eg values are listed in Table 4 for ambient conditions and Table 5 for dehydrated conditions. For the supported MoO_3/Al_2O_3 and MoO_3/SiO_2 catalysts, the Raman spectra reveal that the strong Raman crystalline MoO_3 nanoparticle (NP) band at ~820 cm^{-1} is essentially absent and that the supported molybdena phase is 100% dispersed as a two-dimensional surface MoO_x overlayer on these supports. For the supported MoO_3/ZrO_2 catalysts, a bare trace of crystalline MoO_3 is only present for the supported 4% MoO_3/ZrO_2 sample. It is critical to confirm that crystalline MoO_3 NPs are absent in the samples before conducting the corresponding UV−vis DRS measurements because modest amounts of crystalline MoO_3, which possesses a low Eg value, will skew the overall UV−vis DRS measurement for the surface molybdena phase.

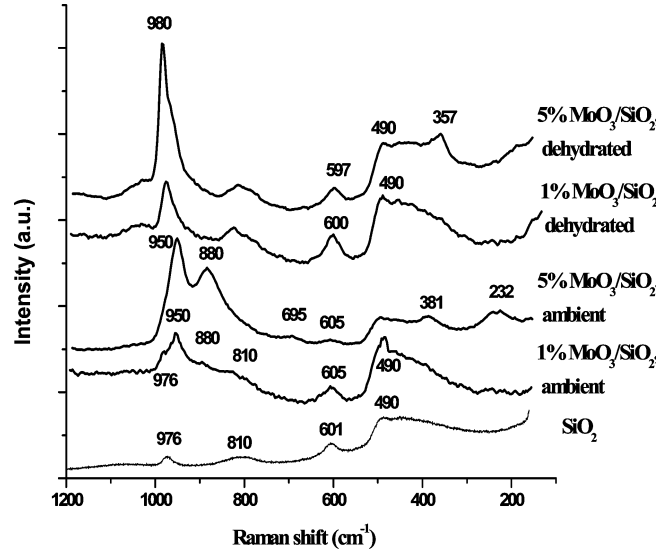

Figure 4. Raman spectra of supported MoO_3/SiO_2 catalysts under ambient and dehydrated conditions as a function of surface molybdena coverage.

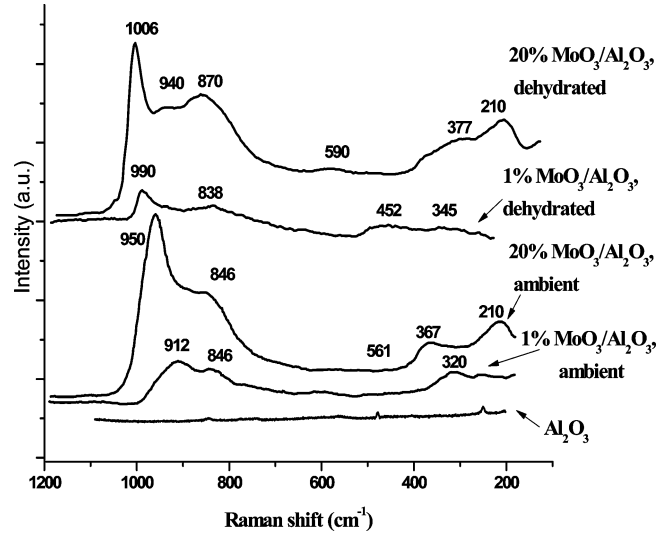

Figure 5. Raman spectra of supported MoO_3/Al_2O_3 catalysts under ambient and dehydrated conditions as a function of surface molybdena coverage.

3.3.1. Ambient Conditions. Under ambient conditions, the surface MoO_x phase is hydrated with moisture, and the surface molybdenum oxide species have been shown to be present in

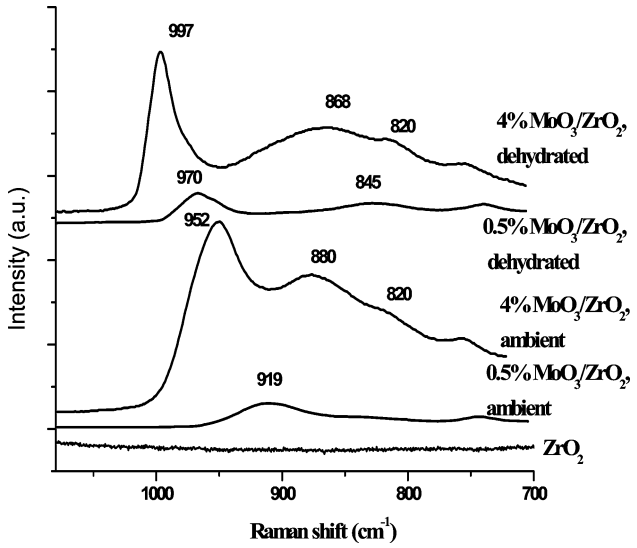

Figure 6. Raman spectra of supported MoO_3/ZrO_2 catalysts under ambient and dehydrated conditions as a function of surface molybdena coverage.

the same molecular structures as found in aqueous molydbdena solutions, the $[Mo_8O_{26}]^{4-}$, $[Mo_7O_{24}]^{6-}$, and $[MoO_4]^{2-}$ anions.[21,32]

MoO_3/SiO_2. For the supported MoO_3/SiO_2 catalysts under ambient conditions, the hydrated surface MoO_x phase gives rise to Raman bands at 950 and 880 cm^{-1} for 1% MoO_3/SiO_2 and 950, 880, ~695, 381, and 232 for 5% MoO_3/SiO_2 as shown in Figure 4. The remaining bands originate from the silica support as can be seen from the Raman spectrum of SiO_2 in Figure 4. The corresponding UV−vis DRS Eg values for both hydrated supported MoO_3/SiO_2 catalysts are listed in Table 4 and are both 3.5 eV. These Eg values match the Eg value previously obtained for the aqueous $[Mo_7O_{24}]^{6-}$ anion (see Table 2). This is further supported by the very similar Raman bands for the aqueous $[Mo_7O_{24}]^{6-}$ cluster (940, 900, 547, 442, 366, and 218 cm^{-1}) and the hydrated supported MoO_3/SiO_2 catalysts (950, 880, 695, 381, and 232 cm^{-1}). The slight differences in position and intensity between the aqueous and silica supported hydrated $[Mo_7O_{24}]^{6-}$ clusters are most probably a consequence of the slight distortion of the anion cluster caused by its interaction with the surface of the SiO_2 support.

MoO_3/Al_2O_3. The Raman spectrum of the hydrated 1% MoO_3/Al_2O_3 catalyst, which corresponds to 0.05 monolayer coverage, is presented in Figure 5 and exhibits bands at 912, 846, and 320 cm^{-1} that fairly well match the Raman bands of the aqueous $[MoO_4]^{2-}$ anion (903, 844, and 326 cm^{-1}). Note that vibrations from bridging Mo−O−Mo bonds are absent. The slight shift of the highest wavenumber band is most probably associated with the distortion of the hydrated, isolated $[MoO_4]^{2-}$ anion on the alumina surface as well as minor amounts of $[Mo_7O_{24}]^{6-}$ anions. Unlike the SiO_2 support, the transitional Al_2O_3 support does not give rise to any Raman bands. The corresponding UV−vis Eg value is listed in Table 4 and is 4.4 eV, which is just below the Eg value of 4.5 eV for the aqueous $[MoO_4]^{2-}$ anion. For the hydrated 20% MoO_3/Al_2O_3 sample, which corresponds to monolayer surface molybdena coverage, very different Raman features are present as shown in Figure 5. The Raman bands for the hydrated 20% MoO_3/Al_2O_3 are present at 950, 846, 501, 367, and 210 cm^{-1}, which most closely match the vibrations of the aqueous $[Mo_7O_{24}]^{6-}$ clusters (940, 900, 547, 442, 366, and 218 cm^{-1}). The corresponding UV−vis DRS Eg value is now much lower and is found at 3.6 eV. This value is only slightly higher than the Eg value of 3.5 eV of the aqueous $[Mo_7O_{24}]^{6-}$ cluster and may reflect the presence of a minor amount of aqueous $[MoO_4]^{2-}$ anion. Thus, unlike the ambient supported MoO_3/SiO_2 catalysts, both hydrated $[MoO_4]^{2-}$ and $[Mo_7O_{24}]^{6-}$ anions are present on the Al_2O_3 support under ambient conditions, and their relative concentration depends on the surface molybdena coverage.

MoO_3/ZrO_2. For the supported MoO_3/ZrO_2 catalysts under ambient conditions, the 0.5% MoO_3/ZrO_2 catalyst, corresponding to 0.13 monolayer coverage, exhibits a Raman band at 919 cm^{-1}, and the supported 4% MoO_3/ZrO_2 catalyst, corresponding to monolayer coverage, exhibits Raman bands at 952 and 880 cm^{-1}. The supported MoO_3/ZrO_2 Raman spectra are not presented in Figure 6 below 700 cm^{-1} because of the strong crystalline ZrO_2 (monoclinic) vibrations that dominate the Raman spectrum in this region. The Raman band position of the hydrated 0.5% MoO_3/ZrO_2 catalyst at 919 cm^{-1} is only consistent with that of the aqueous $[MoO_4]^{2-}$ anion. This is supported by the corresponding UV−vis Eg value listed in Table 4 as 4.4 eV. The slightly lower Eg value relative to the $[MoO_4]^{2-}$ anion at 4.5 eV most probably reflects the presence of a small amount of hydrated $[Mo_7O_{24}]^{6-}$ clusters in this sample. The Raman band positions of 952 and 880 cm^{-1} for the hydrated 4% MoO_3/ZrO_2 reflect the presence of hydrated $[Mo_7O_{24}]^{6-}$ clusters (940 and 900 cm^{-1}). The corresponding UV−vis DRS Eg value is 3.3 eV, which is slightly lower than 3.5 eV expected for the aqueous $[Mo_7O_{24}]^{6-}$ cluster and may reflect the additional presence of some aqueous $[Mo_8O_{26}]^{4-}$ clusters or small experimental error. Similar to the ambient supported MoO_3/Al_2O_3 catalysts that exhibit multiple aqueous molybdena anions with surface molybdena coverage, the ambient supported MoO_3/ZrO_2 catalysts can contain hydrated $[MoO_4]^{2-}$, $[Mo_7O_{24}]^{6-}$, and possibly some $[Mo_8O_{26}]^{4-}$ anions with their relative concentrations depending on the surface molybdena coverage.

3.3.2. Dehydrated Conditions. Upon dehydration, the adsorbed moisture evaporates and the molybdena anions decompose, and the molybdena anchor to the oxide support by titrating the support surface hydroxyls.[21,32]

MoO_3/SiO_2. For the dehydrated supported MoO_3/SiO_2 catalysts (Figure 4), the Raman spectra exhibit a sharp band at 980 cm^{-1} that has been assigned to the isolated dioxo surface $(O{=})_2MoO_2$ species,[81−84] and the additional weaker band at 357 cm^{-1} present for the higher loaded sample corresponds to the associated surface MoO_4 bending mode. The absence of the bridging Mo−O−Mo deformation mode at ~220 cm^{-1} is consistent with only the presence of isolated surface MoO_x species on the SiO_2 support under dehydrated conditions.

MoO_3/Al_2O_3. The Raman spectra of the dehydrated supported MoO_3/Al_2O_3 catalysts are presented in Figure 5. The dehydrated supported 1% MoO_3/Al_2O_3 catalyst possessing about 0.05 monolayer coverage exhibits a sharp Raman band at ~990 cm^{-1} that is consistent with the symmetric stretch of dioxo surface $(O{=})_2MoO_4$ species.[81−84] The corresponding bands at ~838 and 345 cm^{-1} are the associated bridging Mo−O−Al stretch and MoO_4 bending modes, respectively. The additional weak, broad band at ~452 cm^{-1} may be the asymmetric MoO_4 bending mode or an anomalous band. For the monolayer covered supported 20% MoO_3/Al_2O_3 catalyst, Raman bands are present at ~1006 (s), ~940 (w), ~870 (m), ~560 (vw), ~377 (m), and ~210 (m) cm^{-1}. The Raman bands at 560 and 210 cm^{-1} arise from the symmetric stretch and bending modes of bridging Mo−O−Mo bonds, respectively.[21] The Raman band at 1006 cm^{-1} coincides with the symmetric stretch found for the monoxo $H_3SiMo_{12}O_{40}$ Keggin,[81] and the band shift from ~990 to 1006 cm^{-1} also coincides with monoxo, surface MoO_5 species from DFT

TABLE 4: Comparison of UV−Vis DRS Local MoO_x Molecular Structural Assignments of Supported MoO_3 Catalysts with Raman and XANES under Ambient Conditions

catalysts	Eg values (eV)	average no. Mo−O−Mo[a]	local MoO_x structural assignments under ambient conditions		
			UV−vis DRS	Raman	XANES[14,21]
1% MoO_3/SiO_2	3.5	∼2.7	$[Mo_7O_{24}]^{6-}$ cluster	$[Mo_7O_{24}]^{6-}$ cluster	MoO_6
5% MoO_3/SiO_2	3.5	∼2.7	$[Mo_7O_{24}]^{6-}$ cluster	$[Mo_7O_{24}]^{6-}$ cluster	MoO_6
1% MoO_3/Al_2O_3	4.4	∼0.4	isolated $[MoO_4]^{2-}$ and trace of $[Mo_7O_{24}]^{6-}$	isolated $[MoO_4]^{2-}$	MoO_4
20% MoO_3/Al_2O_3	3.6	∼2.4	$[Mo_7O_{24}]^{6-}$ cluster and trace of isolated $[MoO_4]^{2-}$	$[Mo_7O_{24}]^{6-}$ cluster	MoO_6
0.5% MoO_3/ZrO_2	4.4	∼0.4	isolated $[MoO_4]^{2-}$ and trace of $[Mo_7O_{24}]^{6-}$	$[MoO_4]^{2-}$ cluster	
4% MoO_3/ZrO_2	3.3	∼3.2	$[Mo_7O_{24}]^{6-}$ cluster and trace of $[Mo_8O_{26}]^{4-}$	$[Mo_7O_{24}]^{6-}$ cluster	

[a] Average number of Mo−O−Mo bonds approximated using eq 1.

TABLE 5: Comparison of UV−Vis DRS Local MoO_x Molecular Structural Assignments of Supported MoO_3 Catalysts with Raman and XANES under Dehydrated Conditions

catalysts	Eg values (eV)	average no. Mo−O−Mo[a]	local MoO_x structural assignments under dehydrated conditions		
			UV−vis DRS	Raman	XANES[14,21]
1% MoO_3/SiO_2	4.4	∼0.4	monomolybdate	monomolybdate $(O{=})_2MoO_2$	MoO_4
5% MoO_3/SiO_2	4.4	∼0.4	monomolybdate	monomolybdate $(O{=})_2MoO_2$	MoO_4
1% MoO_3/Al_2O_3	4.4	∼0.4	monomolybdate	monomolybdate $(O{=})_2MoO_2$	MoO_4
20% MoO_3/Al_2O_3	4.1	∼1.4	monomolybdate and polymolybdate	polymolybdate $O{=}MoO_4$	MoO_4 and MoO_6
0.5% MoO_3/ZrO_2	4.4	∼0.4	monomolybdate	monomolybdate $(O{=})_2MoO_2$	
4% MoO_3/ZrO_2	4.0	∼1.4	monomolybdate and polymolybdate	polymolybdate $O{=}MoO_4$	

[a] Average number of Mo−O−Mo bonds approximated using eq 1.

calculations.[83,84] The Raman band at ∼870 cm^{-1} is associated with the bridging Mo−O−Al stretch, and the remaining bands at ∼940 and 377 cm^{-1} are related to the asymmetric stretch and bending mode of the polymeric surface MoO_5 species. Thus, unlike the dehydrated supported MoO_3/SiO_2 catalysts that only contain isolated surface MoO_x species, both isolated and polymeric dehydrated surface MoO_x species are present on Al_2O_3, and their relative concentration depends on the surface MoO_x coverage.

MoO_3/ZrO_2. The Raman spectra of the dehydrated supported MoO_3/ZrO_2 catalysts are shown in Figure 6. The dehydrated supported 0.5% MoO_3/ZrO_2 catalyst, which contains ∼0.13 monolayer MoO_x coverage, exhibits Raman bands at ∼970 and ∼845 cm^{-1}. The Raman band at 970 cm^{-1} is assigned to the symmetric stretch of dioxo surface $(O{=})_2MoO_2$ species,[80−84] and the weak band at ∼845 cm^{-1} is the vibration from the bridging Mo−O−Zr bond. The Raman band shift from ∼970 to 997 cm^{-1} from the dehydrated supported 1% to 4% MoO_3/ZrO_2 catalysts is consistent with transformation of dioxo surface $(O{=})_2MoO_2$ species to monoxo $O{=}MoO_4$ species at monolayer coverage.[83,84] The bridging Mo−O−Zr vibration occurs at ∼868 cm^{-1}, and the weak band at ∼820 cm^{-1} is from a trace of crystalline MoO_3 NPs. Note that the Raman cross-section for crystalline MoO_3 is more than an order of magnitude greater than that of the surface MoO_x species and, consequently, is very easy to detect with Raman. The inability to detect MoO_x vibrations below 700 cm^{-1}, due to the strong ZrO_2 Raman vibrations in this region, prevents determination of the extent of polymerization of the dehydrated surface MoO_x species on the ZrO_2 support.

3.3.3. Quantitative Determination of Polymerization Extent of Dehydrated Surface Molybdena Species. The extent of polymerization of the dehydrated surface MoO_x species was estimated by interpolating the UV−vis Eg values between that of the isolated, aqueous $[MoO_4]^{2-}$ anion (Eg = 4.5 eV) and linear chains of alternating MoO_4/MoO_6 units present in bulk $(NH_4)_2Mo_2O_7$ (Eg = 3.5 eV) as was previously performed for analogous vanadium oxide structures.[85] The MoO_x clusters were not considered in this determination because they possess 3D morphology, and the dehydrated surface MoO_x are only present as 1D and 2D configurations. It should also be noted that due to the broad nature of UV−vis bands, individual bands for monomers and polymers are not present; rather a single leading edge yielding an Eg indicative of the extent of polymerization was found (see Figure S2). For the low surface coverage supported MoO_3 catalysts under dehydrated conditions, such an estimate suggests that ∼90% of the dehydrated surface MoO_x species are isolated on the different oxide supports. These values may be slightly affected by the broader UV−vis DRS bands for the dehydrated surface MoO_x species as compared to the reference compounds of aqueous $[MoO_4]^{2-}$ and crystalline $(NH_4)_2Mo_2O_7$. For the monolayer covered supported MoO_3 catalysts under dehydrated conditions, the estimate suggests ∼60% monomer (∼40% polymer) for the supported MoO_3/Al_2O_3 catalyst and ∼35% monomer (∼65% polymer) for the supported MoO_3/ZrO_2 catalyst. Thus, in agreement with the above Raman observations, essentially only dehydrated, isolated surface MoO_x species are present on all of the oxide supports at low surface MoO_x coverage, which also includes the maximum surface MoO_x coverage on SiO_2 because of its low coverage. The monolayer-covered supported MoO_3/Al_2O_3 and MoO_3/ZrO_2 catalysts, however, possess ∼40% and ∼65% polymeric surface MoO_x species, respectively, indicating greater extent of polymerization on ZrO_2 than Al_2O_3.

4. Discussion

4.1. Correlation of the UV−Vis DRS Eg with the Local Structures of Mo(VI) Oxides. The successful correlation of the number of M−O−M bonds or the local symmetry of the central cation with the UV−vis DRS edge energies for V(V) and W(VI) cations has been previously reported.[51,86] Furthermore, an attempt to correlate domain size and edge energy using data from several sources has already been made.[48] Following the previous successful empirical correlations between Eg and the number of nearest cations surrounding the central M cation, a correlation between Eg and the average number of covalent bridging Mo−O−Mo bonds ($N_{Mo-O-Mo}$) of the central Mo(VI) cation is also examined for the Mo(VI)-containing molybdenum oxide reference compounds investigated in this Article. The plot of $N_{Mo-O-Mo}$ versus Eg is presented in Figure 7, where the Eg

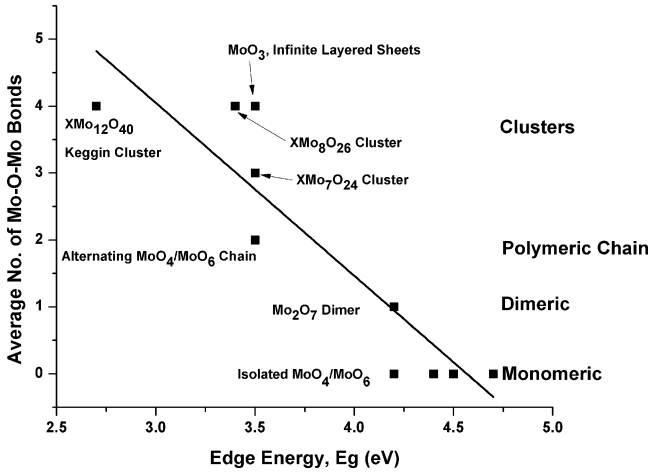

Figure 7. Correlation between the UV−vis DRS edge energy (Eg) and number of bridging Mo−O−Mo bonds in bulk mixed-metal molybdates, ammonium salts, and aqueous solution molybdena anions present in the different Mo(VI) structures.

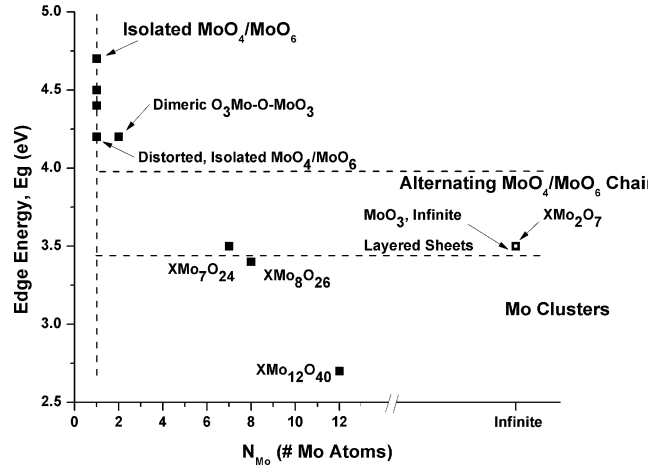

Figure 8. Correlation between the UV−vis DRS edge energy and the number of Mo atoms (N_{Mo}) present in bulk molybdate reference compounds.

values have an inverse linear variation with $N_{Mo-O-Mo}$, with the exception of the isolated MoO_x structures whose Eg values vary over a wide range (4.2−4.7 eV) due to distortion, which is similar to the earlier correlations for V(V) and W(VI) compounds.[51] This relationship is quite similar to the correlation proposed by Weber for Mo(VI) compounds, which represents the degree of aggregation/polymerization of the absorbing species.[48] The line shown in Figure 7 can be expressed by the equation:

$$N_{Mo-O-Mo} = 11.8 - 2.6\text{Eg with } R^2 = 0.80 \qquad (1)$$

The high R^2 value is attributed to the distribution of Eg values for the isolated MoO_4/MoO_6 structures due to the distortion of the isolated MoO_x structures that can be observed in the Raman spectra. The obtained Mo(VI) correlation is comparable to that obtained by Weber for Mo(VI) oxide clusters, $N_{Mo} = 16 - 3.8\text{Eg}$. However, Weber obtained his Eg values from multiple publications, whereas the current study generated a consistent set of Eg values. There is also a striking similarity to the correlations found by Gao et al. for V(V) oxide clusters, $N_{V-O-V} = 14.03 - 3.95\text{Eg}$, and by Ross-Medgaarden et al. for W(VI) oxide clusters, $N_{W-O-W} = 11.89 - 2.37\text{Eg}$. The similar correlations obtained for the Mo(VI), V(VI), and W(V) cations suggest that the edge energies of metal oxide clusters are associated with the extent of spatial delocalization of the molecular orbitals involved with electronic transitions, as initially proposed by Weber.[48] It follows from the correlation in Figure 7 that Eg is primarily determined by the number of covalent bridging Mo−O−Mo bonds or the degree of polymerization of the central Mo(VI) cation. The wide range of Eg values obtained for the isolated MoO_4/MoO_6 structures appears to reflect the sensitivity of the UV−vis DRS measurement to the extent of distortion of the Mo(VI) cation and needs to be considered when determining local structures.

An inverse relationship between Eg and domain size or number of MoO_x units in a molybdenum oxide cluster or domain size has also recently been invoked in the literature, but never been rigorously examined.[5] The plot of Eg versus N_{Mo}, where N_{Mo} represents the number of Mo atoms present in a finite cluster, is presented in Figure 8. The Eg versus N_{Mo} plot does not support a direct relationship between Eg and N_{Mo} or domain size for finite MoO_x clusters as shown by the plot in Figure 8. First, the Eg values for isolated MoO_4/MoO_6 structures vary over a very wide range due to the sensitivity to extent of distortion of the Mo(VI) cation. Second, comparable Eg values are obtained for finite Mo_7 and Mo_8 clusters and infinite linear chains. It is also obvious that the bulk crystal structure of MoO_3 containing infinite sheets of Mo atoms does not fall within this trend as it too has an Eg value similar to an infinite linear chain or finite cluster. The position of the infinite sheets in the bulk crystal correlates well with the infinite polymeric chain (XMo_2O_7); however, the polymeric chain's point also does not fall within the trend invoked in the literature. The inverse relationship between Eg and number of Mo−O−Mo bonds in Figure 7 better captures the variation of the UV−vis DRS Eg values with the local structure of the Mo(VI) cation.

4.2. Aqueous Polymolybdates as a Function of Solution pH. The presence of three distinct aqueous molybdena species ($[MoO_4]^{2-}$, $[Mo_7O_{24}]^{6-}$ and $[Mo_8O_{26}]^{4-}$) were detected as a function of pH for a 0.2 M $(NH_4)_6Mo_7O_{24}$ solution and the corresponding Raman spectra and UV−vis Eg values were shown to correspond to their respective ammonium salts. As pH was decreased from 9.27 to 2.95 the aqueous molybdena species began as $[MoO_4]^{2-}$ at the highest pH and transitioned through $[Mo_7O_{24}]^{6-}$ species before ultimately existing as $[Mo_8O_{26}]^{4-}$ species at the lowest pH. The effect of pH on molybdena-containing sample preparation has been previously studied by Williams et al. and the current study is in agreement with those findings.[26] More recently, Bergwerff et al. have performed nearly identical studies on 0.1 M $(NH_4)_6Mo_7O_{24}$ solutions.[87−89] Their results showed that the three aqueous molybdena species are present within approximately the same pH ranges found in the current study as confirmed by similar Raman band assignments. Furthermore, their studies showed well the applicability of such a pH study to the actual structure of molybdena species on support materials.

4.3. Surface Structures of Supported Molybdenum Oxide Catalysts under Ambient Conditions. Only the aqueous $[MoO_4]^{2-}$, $[Mo_7O_{24}]^{6-}$, or $[Mo_8O_{26}]^{4-}$ anions are present on the hydrated supported MoO_3 catalysts, and their relative surface concentrations depend on the overall surface pH at PZC (point of zero charge) of the catalyst system.[21,90] The hydrated isolated $[MoO_4]^{2-}$ species are primarily present at low surface coverage on the Al_2O_3 and ZrO_2 support, which correspond to higher pH at PZC conditions (see UV−vis DRS, Table 2).[21,90] The hydrated $[Mo_7O_{24}]^{6-}$ cluster is primarily present at intermediate pH at

PZC values (see UV−vis DRS, Table 2) and is present at monolayer coverage on the hydrated Al_2O_3 and ZrO_2 supports. The slightly lower UV−vis Eg value for the hydrated monolayer of surface MoOx on ZrO_2 suggests that some $[Mo_8O_{26}]^{4-}$ anions are probably also present for this catalyst system. The hydrated supported MoO_3/SiO_2 catalysts only possess the $[Mo_7O_{24}]^{6-}$ anion at all coverage because of the lower pH at PZC of SiO_2 (pH at PZC ≈ 2−4) relative to the Al_2O_3 (pH at PZC = 9) and ZrO_2 (pH at PZC = 6) supports.[90] These UV−vis DRS assignments are in excellent agreement with the corresponding Raman assignments for the hydrated supported MoO_3 catalysts (see Table 4). The UV−vis and Raman assignments are also consistent with earlier reported XANES analysis that readily discriminates between MoO_4 and MoO_6 coordination (see Table 4). Among the three spectroscopic characterization techniques, it appears that the UV−vis Eg value is more sensitive than Raman and XANES for detecting small concentrations of secondary species. Thus, hydrated $[MoO_4]^{2-}$ and $[Mo_7O_{24}]^{6-}$ anions are primarily present in supported MoO_3 catalysts under ambient conditions, and their relative concentrations depend on the overall pH at surface PZC, which is dependent on the oxide support PZC and the surface MoO_x coverage (MoO_3 PZC ≈ 2).[21]

The current conclusions for hydrated supported MoO_3 catalysts are in excellent agreement with earlier Raman and XANES measurements for the hydrated supported MoO_3/SiO_2, MoO_3/Al_2O_3, and MoO_3/Nb_2O_5 systems.[21] The earlier investigation also examined the supported MoO_3/TiO_2 and MoO_3/Nb_2O_5 systems that gave the same results for the hydrated MoO_x molecular structures as a function of surface molybdate coverage on the supports. This shows that these hydrated molybdate structures are universal and will be present for all types of supported molybdenum oxide catalysts under ambient conditions as a function of surface MoO_x coverage.

4.4. Surface Structures of Supported Molybdenum Oxide Catalysts under Dehydrated Conditions. The hydrated molybdate anions do not survive thermal dehydration treatments and become directly coordinated to the oxide support surface upon the desorption of moisture.[21,32] This is reflected in the decrease in number of bridging Mo−O−Mo bonds that is ∼3 for the hydrated $[Mo_7O_{24}]^{6-}$ cluster on the supports that decreases upon dehydration to ∼0.3−0.4 on SiO_2, ∼1.1 on Al_2O_3, and ∼1.3 on ZrO_2 at maximum dispersion (see Tables 4 and 5). The isolated dioxo surface $(O{=})_2MoO_2$ species predominate at low surface coverage on all of the dehydrated oxide supports as reflected in their low number of Mo−O−Mo bonds (0.3−0.4). At monolayer coverage, both surface monomolybdate dioxo $(O{=})_2MoO_2$ and polymolybdate monoxo $O{=}MoO_4$ structures coexist on the dehydrated Al_2O_3 and ZrO_2 supports with the concentration of polymolybdates greater on zirconia than on alumina (number of Mo−O−Mo bonds ∼1.1−1.3). The Raman spectra of the dehydrated supported MoO_3 catalysts appear to be dominated by the most abundant surface molybdate species and especially the surface polymolybdates when present. In contrast, XANES detects the presence of both the dehydrated surface MoO_4 and surface MoO_6, or MoO_5, species. UV−vis DRS, however, is most sensitive to the simultaneous presence of dehydrated surface monomolybdate and polymolybdate species. Nevertheless, the different spectroscopic probes are in agreement with regards to the structural nature of the dehydrated surface molybdate species.

The current conclusions for dehydrated supported MoO_3 catalysts are in excellent agreement with earlier in situ Raman and XANES measurements for the dehydrated supported MoO_3/SiO_2, MoO_3/Al_2O_3, and MoO_3/Nb_2O_5 systems.[21] The earlier investigation also examined the dehydrated supported MoO_3/TiO_2 and MoO_3/Nb_2O_5 systems. The dehydrated surface MoO_x species on TiO_2 were primarily present as isolated MoO_4 species at low coverage and polymolybdate MoO_6 species at high coverage based on in situ XANES and Raman spectroscopic analysis. Although in situ XANES data were not collected for dehydrated supported MoO_3/Nb_2O_5, the corresponding in situ Raman spectra suggested the same dehydrated surface MoO_x species are present on Nb_2O_5 as a function of surface coverage. Thus, the dehydrated surface MoO_x species on oxide supports follow a general pattern: isolated, dioxo surface $(O{=})_2MoO_2$ species at low surface coverage and polymolybdate, monoxo $O{=}MoO_4$ at high surface coverage. The ratio of dehydrated polymolybdates/monomoloybdates increases with surface coverage and also depends on the specific oxide support ($SiO_2 < Al_2O_3 < ZrO_2 \approx TiO_2 \approx Nb_2O_5$). These general trends hold for all dehydrated supported MoO_x catalysts as long as the surface MoO_x species do not undergo reaction with the bulk of the oxide support (e.g., supported MoO_3/MgO forms $MgMoO_4$).

The vibrational assignments for dehydrated surface monoxo $O{=}MoO_4$ and dioxo $(O{=})_2MoO_2$ species on SiO_2 have been called into question on the basis of recent density functional theory (DFT) calculations.[91] The recent DFT study calculated the Raman active vibrations for model isolated molybdenum oxide centers (oxo- and dioxo-molybdasilsesquioxanes) on SiO_2 and concluded that the earlier vibrational assignments for the symmetric stretch vibrations of monoxo and dioxo MoO_x species should be reversed (monoxo Mo=O at 989 cm^{-1} and dioxo $(O{=})_2Mo$ at 1005 cm^{-1}). The recent DFT calculation predicts that the asymmetric stretch of the dioxo surface $(O{=})_2MoO_2$ species should occur at ∼965−975 cm^{-1}, which is indeed experimentally observed.[91,92] A prior more detailed DFT study of supported molybdena−silica systems by Handzlik has shown that the current experimental assignments are indeed in agreement with the theoretical results.[93] Rather than using clusters, Handzlik modeled the silica surface as a fragment containing 15 Si atoms that were cut out from a β-cristobalite structure. Using this unit, the calculated dioxo $(O{=})_2Mo$ stretching frequency was found to be at 983 cm^{-1} for the dehydrated surface dioxo species, and the Mo=O stretch of the surface monoxo species is at 1008 cm^{-1}. Thus, the original vibrational assignments for dehydrated supported monoxo and dioxo surface MoO_x species on SiO_2 are in agreement with the more detailed Handzlik study, and the Raman band at 1020 cm^{-1} arises from the dehydrated monoxo surface $O{=}MoO_4$ species.

5. Conclusions

On the basis of well-defined molybdates in bulk oxide reference compounds and aqueous solutions as a function of pH, a correlation of $N_{Mo-O-Mo} = 11.83 - (2.61)Eg$ was established between the edge energy, Eg, and the average number of covalent Mo−O−Mo bonds around the central Mo(VI) cations. A direct relationship between Eg and N_{Mo}, the number of Mo atoms in a molybdate cluster, however, was not found to exist.

Application of the UV−vis DRS and Raman spectroscopy relationships to supported MoO_3 catalysts allowed for electronic and molecular structural determination of the dispersed surface MoO_x phase on oxide supports under ambient and dehydrated conditions. Under ambient conditions, only the hydrated $[MoO_4]^{2-}$, $[Mo_7O_{24}]^{6-}$, and $[Mo_8O_{26}]^{4-}$ anions are present on the oxide supports, and their relative concentrations depend on the pH at PZC of the oxide support and the surface molybdenum

oxide density. The aqueous $[MoO_4]^{2-}$ anion is the major species at low surface coverage on the hydrated Al_2O_3 and ZrO_2 supports. The aqueous $[Mo_7O_{24}]^{6-}$ cluster is predominant on the hydrated SiO_2 and at monolayer coverage on Al_2O_3 and ZrO_2 supports. A trace of aqueous $[Mo_8O_{26}]^{4-}$ may also coexist at monolayer coverage on the hydrated ZrO_2 support. Under dehydrated conditions, where surface moisture is absent, monomolybdate surface $(O{=})_2MoO_2$ species predominate at low surface coverage and both monomolybdate $(O{=})_2MoO_2$ and polymolybdate $O{=}MoO_4$ surface species at monolayer surface coverage.

The above electronic and molecular structural findings are critical for studies that wish to establish reliable structure−activity/selectivity relationships for molybdenum oxide catalysts, especially supported MoO_3 catalysts.

Acknowledgment. This research was financially supported by the Department of Energy-Basic Energy Sciences grant DE-FG02-93-ER14350. We gratefully acknowledge H. C. Starck Co. for supplying the molybdena salt reference compounds. This Article is dedicated to the memory of Professor Jerzy Haber (Institute of Catalysis and Surface Chemistry, Polish Academy of Sciences, Krakow, Poland) who was a pioneer in molybdenum oxide catalysis.

Supporting Information Available: Graphs S1 and S2 and their discussions. This material is available free of charge via the Internet at http://pubs.acs.org.

References and Notes

(1) Haber, J. *The Role of Molybdenum in Catalysis*; Climax Molybdenum Co. Ltd.: London, 1981.
(2) Zhen, Z.; Gao, X.; Wachs, I. E. *J. Phys. Chem. B* **2003**, *107*, 6333.
(3) Stern, D. L.; Grasselli, R. K. *J. Catal.* **1997**, *167*, 550.
(4) Watson, R. B.; Ozkan, U. S. *J. Catal.* **2000**, *191*, 12.
(5) Chen, K.; Xie, S.; Iglesia, E.; Bell, A. T. *J. Catal.* **2000**, *189*, 421.
(6) Farneth, W. E.; Staley, R. H.; Domaille, P. H.; Farlee, R. D. *J. Am. Chem. Soc.* **1987**, *109*, 4018.
(7) Briand, L. E.; Baronetti, G. T.; Thomas, H. J. *Appl. Catal., A* **2003**, *256*, 37.
(8) Valle, G. M.; Briand, L. E. *Mater. Lett.* **2003**, *57*, 3964.
(9) Banares, M. A.; Khatib, S. J. *Catal. Today* **2004**, *96*, 251.
(10) Wachs, I. E.; Segawa, K. In *Characterization of Catalytic Materials*; Wachs, I. E., Ed.; Butterworth-Heinemann: Boston, 1992; Vol. 69.
(11) Bartlett, J. R.; Cooney, R. P. In *Spectroscopy of Inorganic-Based Materials*; Clark, R. J. H., Hester, R. E., Eds.; Wiley: New York, 1987; p 187.
(12) Mehicic, M. In *Analytical Raman Spectroscopy*; Grasselli, J. G., Bulkin, B. J., Eds.; Wiley: New York, 1991; p 325.
(13) Stencel, J. M. *Raman Spectroscopy for Catalysis*; Van Norstrand Reinhold: New York, 1990.
(14) Radhakrishnan, R.; Reed, C.; Oyama, S. T.; Seman, M.; Kondo, J. N.; Domen, K.; Ohminami, Y.; Asakura, K. *J. Phys. Chem. B* **2001**, *105*, 8519.
(15) Arena, F.; Paramaliana, A. *J. Phys. Chem.* **1996**, *100*, 19994.
(16) Desikan, L.; Huang, L.; Oyama, S. T. *J. Phys. Chem.* **1991**, *95*, 10050.
(17) Liu, T.-C.; Forissier, M.; Coudurier, G.; Vedrine, J. G. *J. Chem. Soc., Faraday Trans.* **1989**, *85*, 1607.
(18) Marcinkowska, K.; Rodrigo, L.; Kaliaguine, S.; Roberge, P. C. *J. Mol. Catal.* **1985**, *33*, 189.
(19) Cordero, R. L.; Gil Lambias, F. J.; Lo'pez Agudo, A. *Appl. Catal.* **1991**, *74*, 125.
(20) Ismail, H. M.; Zaki, M. I.; Bond, G. C.; Shukri, R. *Appl. Catal.* **1991**, *72*, L1.
(21) Hu, H.; Wachs, I. E.; Bare, S. R. *J. Phys. Chem.* **1995**, *99*, 10897.
(22) Shimada, H.; Matsubayashi, N.; Sato, T.; Yoshimura, Y.; Nishijama, A.; Kosugi, N.; Kuroda, H. *J. Catal.* **1992**, *138*, 746.
(23) Ng, K. Y. S.; Zhou, X.; Gulari, E. *J. Phys. Chem.* **1985**, *89*, 2477.
(24) Payen, E.; Grimblot, J.; Kasztelan, S. *J. Phys. Chem.* **1987**, *91*, 6642.
(25) Kohler, S. D.; Ekerdt, J. G.; Kim, D. S.; Wachs, I. E. *Catal. Lett.* **1992**, *16*, 231.
(26) Williams, C. C.; Ekerdt, J. G.; Jehng, J.-M.; Hardcastle, F. D.; Wachs, I. E. *J. Phys. Chem.* **1991**, *95*, 8791.
(27) Vuurman, M. A.; Wachs, I. E. *J. Phys. Chem.* **1992**, *96*, 5008.
(28) Vuurman, M. A.; Wachs, I. E. *J. Mol. Catal.* **1992**, *77*, 29.
(29) Gao, X.; Xin, Q. *Catal. Lett.* **1993**, *18*, 409.
(30) Diaz, A. L.; Bussell, M. E. *J. Phys. Chem.* **1993**, *97*, 470.
(31) Smith, M. R.; Zhang, L.; Driscoll, S. A.; Ozkan, U. S. *Catal. Lett.* **1993**, *19*, 1.
(32) Kim, D. S.; Segawa, K.; Soeya, T.; Wachs, I. E. *J. Catal.* **1992**, *136*, 539.
(33) Martin, C.; Martin, M.; Rives, V. *Stud. Surf. Sci. Catal.* **1992**, *72*, 415.
(34) de Boer, M.; van Dillen, A. J.; Koningsberger, D. C.; Geus, J. W.; Vuurman, M. A.; Wachs, I. E. *Catal. Lett.* **1991**, *16*, 71.
(35) Williams, C. C.; Ekerdt, J. G.; Jehng, J.-M.; Hardcastle, F. D.; Turek, A. M.; Wachs, I. E. *Catal. Lett.* **1991**, *95*, 8781.
(36) Roark, R. D.; Kohler, S. D.; Ekerdt, J. G.; Kim, D. S.; Wachs, I. E. *Catal. Lett.* **1992**, *16*, 77.
(37) Roark, R. D.; Kohler, S. D.; Ekerdt, J. G. *Catal. Lett.* **1992**, *16*, 71.
(38) Banares, M. A.; Fierro, J. L. G. *Catal. Lett.* **1993**, *17*, 205.
(39) Aigler, J. M.; Brito, J. L.; Leach, P. A.; Houalla, M.; Proctor, A.; Cooper, N. J.; Hall, W. K.; Hercules, D. M. *J. Phys. Chem.* **1993**, *97*, 5699.
(40) Louis, C.; Che, M. *J. Catal.* **1992**, *135*, 156.
(41) Ono, T.; Miyata, H.; Kubokawa, Y. *J. Chem. Soc., Faraday Trans. 1* **1987**, *83*, 1761.
(42) Miyata, H.; Tokuda, S.; Ono, T.; Ohno, T.; Hatayama, F. *J. Chem. Soc., Faraday Trans. 1* **1990**, *86*, 2291.
(43) Weckhuysen, B. M.; Schnoonheydt, R. A. *Catal. Today* **1999**, *49*, 441.
(44) Kim, Y. I.; Rily, R. L.; Huq, M. J.; Salim, S.; Le, A. N.; Mallouk, T. E. *Mater. Res. Soc. Symp. Proc.* **1991**, *233*, 145.
(45) Hoener, C. F.; Allan, K. A.; Bard, A. J.; Campion, A.; Fox, M. A.; Mallouk, T. E.; Webber, S. E.; White, J. M. *J. Phys. Chem.* **1992**, *96*, 3812.
(46) Davis, R. J. *Chem. Mater.* **1992**, *4*, 1410.
(47) Liu, Z.; Davis, R. J. *J. Phys. Chem.* **1994**, *98*, 1253.
(48) Weber, R. S. *J. Catal.* **1995**, *151*, 470.
(49) Briand, L. E.; Hirt, A. M.; Wachs, I. E. *J. Catal.* **2001**, *202*, 268.
(50) Burcham, L. J.; Briand, L. E.; Wachs, I. E. *Langmuir* **2001**, *17*, 6175.
(51) Gao, X.; Wachs, I. E. *J. Phys. Chem. B* **2000**, *104*, 1261.
(52) Hardcastle, F. D.; Wachs, I. E. *J. Raman Spectrosc.* **1990**, *21*, 683.
(53) Ponceblanc, H.; Millet, J. M.; Herrmann, J. M. *J. Catal.* **1993**, *142*, 373.
(54) Hill, C. G.; Wilson, J. H. *J. Mol. Catal.* **1990**, *63*, 65.
(55) Kovats, W. D.; Hill, C. G. *Appl. Spectrosc.* **1986**, *40*, 1215.
(56) Mestl, G. *J. Raman Spectrosc.* **2002**, *33*, 333.
(57) Jehng, J.-M.; Wachs, I. E.; Clark, F. T.; Springman, M. C. *J. Mol. Catal.* **1993**, *81*, 63.
(58) Forzatti, P.; Mari, C. M.; Villa, P. *Mater. Res. Bull.* **1987**, *22*, 1593.
(59) Hardcastle, F. D.; Wachs, I. E. *J. Phys. Chem.* **1991**, *95*, 10763.
(60) Chang, S. C.; Leugers, M. A.; Bare, S. R. *J. Phys. Chem.* **1992**, *96*, 10358.
(61) Machida, N.; Echert, H. *Solid State Ionics* **1998**, *107*, 255.
(62) Ozkan, U. S.; Schrader, G. L. *J. Catal.* **1985**, *95*, 120.
(63) Saleem, S. S. *Infrared Phys.* **1987**, *27*, 309.
(64) Wiesmann, M. E.; Wltschek, G.; Zinn, P.; Weitzel, H.; Fuess, H. *J. Magn. Magn. Mater.* **1995**, *150*, L1.
(65) Rodriguez, J. A.; Chaturvedi, S.; Hanson, J. C.; Albornoz, A.; Brito, J. L. *J. Phys. Chem. B* **1998**, *102*, 1347.
(66) Less, J. D.; Bardin, B. B.; Kim, H. S.; Ko, D.; Smith, M. T.; Hammond, R. R.; Stair, P. C.; Poeppelmeier, K. R. *J. Catal.* **2004**, *223*, 419.
(67) Tadnicka, K.; Haber, J.; Kozlowski, R. *Acta Crystallogr., Sect. B* **1977**, *B33*, 3859.
(68) Knopnadel, I.; Hartl, H.; Hunnius, W. D.; Fuchs, J. *Angew. Chem., Int. Ed. Engl.* **1974**, *13*, 823.
(69) Gatehouse, B. M. *J. Less-Common Met.* **1974**, *36*, 53.
(70) Knoepnadel, I.; Hartl, H.; Hunnius, W. D.; Fuchs, J. *Angew. Chem.* **1974**, *86*, 894.
(71) Fuchs, J.; Hartl, H.; Hunnius, W. D.; Mahjour, S. *Angew. Chem.* **1975**, *87*, 634.
(72) Liu, G.; Zhang, S. W.; Tang, Y. Q. *Z. Anorg. Allg. Chem.* **2001**, *627*, 1077.
(73) Parimal, K.; Bharadwaj, Y. O.; Yoshio, S.; Yoh, S.; Toshihiro, Y. *Acta Crystallogr.* **1986**, *C42*, 545.
(74) Bridgeman, A. *J. Chem. Phys.* **2003**, *287*, 55.
(75) Kasprzak, M. S.; Crouch, S. R.; Leroi, G. E. *Appl. Spectrosc.* **1978**, *32*, 537.
(76) Bridgeman, A. J. *Chem.-Eur. J.* **2004**, *10*, 2935.
(77) Kuroiwa, Y.; Sato, N.; Sawada, A.; Negishi, S.; Negishi, H.; Aoyagi, S. *J. Phys. Soc. Jpn.* **2003**, *72*, 2811.

(78) Seguin, L.; Figlarz, M.; Cavagnat, R.; Lasskgues, J.-C. *Spectrochim. Acta, Part A* **1995**, *51*, 1323.
(79) Ng, K. Y. S.; Gulari, E. *Polyhedron* **1984**, *3*, 1001.
(80) Fournier, M.; Louis, C.; Che, M.; Chaquin, P.; Masure, D. *J. Catal.* **1989**, *119*, 400.
(81) Lee, E. L.; Wachs, I. E. *J. Phys. Chem. C* **2007**, *111*, 14410.
(82) Wang, Y.; Mahler, S. W.; Kasowski, R. *J. Chem. Phys.* **1987**, *87*, 7316.
(83) Chempath, S.; Zhang, Y.; Bell, A. T. *J. Phys. Chem. C* **2007**, *111*, 1291.
(84) Handzlik, J.; Sautet, P. *J. Phys. Chem. C* **2008**, *112*, 14456.
(85) Tian, H.; Ross, E. I.; Wachs, I. E. *J. Phys. Chem. B* **2006**, *110*, 9593.
(86) Ross-Medgaarden, E. I.; Wachs, I. E. *J. Phys. Chem. C* **2007**, *111*, 15089.
(87) Bergwerff, J. A.; Visser, T.; Weckhuysen, B. M. *Catal. Today* **2008**, *130*, 117.
(88) Bergwerff, J. A.; Visser, T.; Leliveld, B. R. G.; Rossenaar, B. D.; de Jong, K. P.; Weckhuysen, B. M. *J. Am. Chem. Soc.* **2004**, *126*, 14548.
(89) Bergwerff, J. A.; Jansen, M.; Leliveld, B. R. G.; Visser, T.; de Jong, K. P.; Weckhuysen, B. M. *J. Catal.* **2006**, *243*, 292.
(90) Deo, G.; Wachs, I. E. *J. Phys. Chem.* **1991**, *95*, 5889.
(91) Gregoriades, L. J.; Döbler, J.; Sauer, J. *J. Phys. Chem. C* **2010**, *114*, 2967.
(92) Lee, E. L.; Wachs, I. E. *J. Phys. Chem. C* **2008**, *112*, 6487.
(93) Handzlik, J. *Chem. Phys. Lett.* **2009**, *469*, 140.

JP103269W